DOI:
10.1002/adom.201801420

Document Version
Peer reviewed version

DOI: 10.1002/((please add manuscript number))
Article type: Full Paper

Magneto-optical metamaterials: Nonreciprocal transmission and Faraday effect enhancement

*Bo Fan, Mazhar E. Nasir, Luke H. Nicholls, Anatoly V. Zayats, and Viktor A, Podolskiy**

Dr. B. Fan
Department of Physics and Applied Physics, University of Massachusetts Lowell, Lowell, MA, 01854, USA

M.E. Nasir, L.H. Nicholls, Prof. A.V. Zayats
Department of Physics and London Centre for Nanotechnology, King's College London, Strand, London, WC2R 2LS, UK
E-mail: a.zayats@kcl.ac.uk

Prof. V.A. Podolskiy
Department of Physics and Applied Physics, University of Massachusetts Lowell, Lowell, MA, 01854, USA
E-mail: viktor_podolskiy@uml.edu

Keywords: (metamaterials, nonreciprocity, Faraday effect, effective medium theory)

Magneto-optical effects are at the heart of modern technologies providing opportunities for polarization control in laser physics and optical communications, metrology and in high-density data storage. Here we developed a new type of a hyperbolic magneto-optical metamaterial based on Au-Ni nanorod arrays. The metamaterial exhibits an enhanced magneto-optical response with large rotation of the polarization plane and nonreciprocal light transmission. We proposed and validated the effective medium model that incorporates both plasmonic and magneto-optical phenomena in complex multi-component nanorod media. The experimental and theoretical results indicate that the magneto-optical response of the nanostructured metamaterial is drastically enhanced and spectrally modified with respect to bulk ferromagnetic media due to interplay between strong anisotropy and magnetic-field induced polarization rotation.

1. Introduction

Magneto-optical effects are at the core of polarization-control, telecommunications, sensing, and the emerging field of non-reciprocal photonics [1,2] where axial symmetry of the magnetic field is the enabling mechanism for the violation of Parity-Time symmetry of the optical response. Unfortunately, homogeneous materials available in nature exhibit relatively weak magneto-optical activity. Artificial magneto-optical behavior has been recently demonstrated in photonic-crystal-inspired structures and in waveguided geometries [3,4], configurations known for their sensitivity to long-range order and, therefore, highly susceptible to fabrication imperfections. Planar multilayered and more complex geometries have been suggested theoretically [5].

Here, we demonstrate that multi-component nanostructured metamaterials can be used to significantly enhance magneto-optical response of their inclusions by combining field enhancement, enabled by plasmonic nanostructures, and the strong anisotropy of nanorod composites [6,7]. The metamaterial is fabricated using standard electrodeposition protocols [8] and operates in the effective medium regime, known for its tolerance to small-scale geometry variations [9,10,12,14,15]. We present comprehensive theoretical, experimental, and numerical analysis of the electromagnetic properties of the magneto-optical metamaterial, demonstrating both the rotation of the polarization plane and non-reciprocal transmission, two phenomena that can be controlled by the direction of the external magnetic field. This enhanced response is the result of the combination of the introduced magneto-optical properties and strong anisotropy of the metamaterial. We demonstrate rotation of the polarization plane with the effective Verdet constant equivalent of at least 10^5 [rad/m/T], significant enhancement with respect to bulk ferromagnetic materials [11], suggesting that nanostructured magnetic materials have much stronger magneto-optical response than their bulk counterparts. Overall, plasmonic magneto-optical nanorods combine the benefits of sub-wavelength light manipulation offered by metamaterials and of strong magneto-optics offered

by plasmonic nanocomposites, leading to a promising material platform for integrated nanophotonic applications.

The magneto-optical metamaterial geometry and its optical response is illustrated in **Figure 1**. The composite is formed by an array of aligned plasmonic (gold) nanorods with magneto-optical (nickel) shells inside a dielectric (alumina) matrix (note that in the composites Ni shells extend only part-way along the rod; see Methods). As follows from the geometry, in the absence of external static magnetic field and in the limit when the unit cell is much smaller than the wavelength ($a \ll \lambda_0$), the optical response of the composite can be described by a diagonal permittivity tensor with Cartesian components $\hat{\epsilon} = \{\epsilon_\perp, \epsilon_\perp, \epsilon_{zz}\}$. Effective medium theory can be used to relate the components of the effective permittivity $\epsilon_\perp$ and ϵ_{zz} to the permittivity of the constituent materials, as well as to the geometrical parameters of a metamaterial, such as a unit cell a, and radii of the rod r_1 and of the shells around the rod r_i, with $i = 2, \dots, N$. Existing analytical and numerical tools allow calculations of the optical response of metamaterials composed of rods without shells, with plasmonic and magneto-optical material constituents and in the limit $r_1 \ll a$ [1,12,15,16], as well as shelled nanorod composites, comprising non-magneto-optical materials with arbitrary rod concentration [13,14]. Here, we present a formalism that can incorporate magneto-optical response in the effective-medium description of shelled rod metamaterials and even in the limit $r_i \simeq \frac{a}{2}$. We consider a metamaterial with a = 64 nm, r_1 = 15 nm and r_2 = 23 nm and assume that the height of each of Ni-clad and air-clad section of the nanorods is equal to 100 nm. Different combinations of geometrical parameters can potentially further optimize magneto-optical response beyond what is reported in this work.

The diagonal components of the effective permittivity (Fig. 1b) are of different signs throughout visible (Au/Ni composites) and IR (Au composite) frequency ranges (see Methods for the details), with poles and resonances of the components of the effective permittivity

resulting in the peaks of optical extinction of the composite (Fig. 1c,d). Metamaterials with such strong anisotropy, also called hyperbolic metamaterials, are known to enable sub-wavelength light manipulation and modulation of optical density of states[9,10,17,18]. This work extends the applications of hyperbolic metamaterials to magneto-optical media, potentially enabling strong magneto-optical activity in sub-wavelength optical waveguides. Magneto-optical media are characterized by the changes in their optical response as result of the applied external magnetic field. The details of these changes are related to the direction and the amplitude of the external magnetic field [19]. In particular, when the external field is perpendicular to the interface, the parallel slab of magneto-optical material rotates the plane of polarization of transmitted light and can be potentially used as an optical isolator [1,2,19].When a magnetic field is parallel to the slab interface and perpendicular to the plane of incidence, a lossy magneto-optical material can result in asymmetric propagation, potentially enabling unidirectional transmission of light [20,21]. In both cases, optical properties of the magneto-optical materials can be related to the non-zero off-diagonal components of their permittivity tensor. For composite materials it becomes important to relate the optical response of the metamaterial constituents to the response of the metamaterial as a whole.

2. Effective medium response of shelled nanorod metamaterials with magneto-optic inclusions

The proposed approach is based on the Maxwell-Garnett-type formalism, extended to high concentration of inclusions [13,14,16]. In contrast to the previous studies, here we implement magneto-optical behavior into the effective medium response of the shelled nanorod composites. The procedure applicable to the case of the anisotropic unit cell and to nanorod materials with multiple shells is described below.

Since the dimensions of the unit cell are much smaller than the free space wavelength ($a \ll \lambda_0$), the quasi-static approximation can be used to calculate the distribution of the electric field across a unit cell of the metamaterial. As such, distribution of the electric field across the unit cell can be related to the solutions of the Laplace equation for the electric potential Φ. In an individual shell, these solutions are represented as

$$\Phi_i(\mathrm{r},\varphi) = \sum_{m=1,3,5,\ldots}^{M}\left(a_{i,m}^{+}r^m + a_{i,m}^{-}\frac{1}{r^m}\right)\cos(m\varphi)$$

$$+\sum_{m=1,3,5,\ldots}^{M}\left(b_{i,m}^{+}r^m + b_{i,m}^{-}\frac{1}{r^m}\right)\sin(m\varphi) + a_{i,0} + b_{i,0}\ln(r) \quad , \qquad (1)$$

where the index i represents the shell number and the index m represents the Fourier index. The problem of finding the effective permittivity of the nanorod composite is, therefore, reduced to the problem of calculating the coefficients of the expansions $\overrightarrow{\alpha_i^{\pm}}$ and $\overrightarrow{\beta_i^{\pm}}$ in each layer, based on the external excitation field that is parameterized by a coefficient $\alpha_{N,1}^{+}$. The procedure of calculating these coefficients is outlined in Methods.

The known potential is used to calculate the distribution of the electric field (in the i^{th} layer $\overrightarrow{E_i} = -\vec{\nabla}\Phi_\mathrm{i}$) and the displacement ($\overrightarrow{D_i} = \widehat{\epsilon_i}\,\overrightarrow{E_i}$) across the unit cell. The components of the effective permittivity tensor are then related to the field distributions via $\langle\vec{D}\rangle = \widehat{\epsilon_{\mathrm{eff}}}\langle\vec{E}\rangle$ with $\langle\cdots\rangle$ being the unit-cell average (note that due to linearity of the Maxwell equations, the effective parameters are independent of the incident electromagnetic field). In calculating the components of the effective permittivity tensor (see Methods), we use the following non-zero tensor components

$$\widehat{\epsilon_{\mathrm{eff},y}} = \begin{pmatrix} \epsilon_\perp & 0 & i\gamma_{xz} \\ 0 & \epsilon_\perp & 0 \\ -i\gamma_{xz} & 0 & \widetilde{\epsilon_{zz}} \end{pmatrix}, \qquad (2a)$$

$$\widehat{\epsilon_{\mathrm{eff},z}} = \begin{pmatrix} \widetilde{\epsilon_\perp} & i\gamma_{xy} & 0 \\ -i\,\gamma_{xy} & \widetilde{\epsilon_\perp} & 0 \\ 0 & 0 & \epsilon_{zz} \end{pmatrix}, \qquad (2b)$$

for an external static magnetic field oriented along $\hat{y}$ and $\hat{z}$ directions, respectively. The diagonal components of the effective permittivity tensors ($\epsilon_\perp, \widetilde{\epsilon_\perp}, \epsilon_{zz}, \widetilde{\epsilon_{zz}}$) represent the material response with the induced polarization along the direction of the external electric field. The off-diagonal components (γ_{xz}, γ_{xy}), responsible for magneto-optical activity, represent the component of the displacement field which is perpendicular to the excitation field. In the absence of an external static magnetic field, we recover $\gamma_{xz} = \gamma_{xy} = 0, \epsilon_\perp = \widetilde{\epsilon_\perp}, \epsilon_{zz} = \widetilde{\epsilon_{zz}}$ with $\epsilon_\perp$ and ϵ_{zz} given by the (modified) Maxwell-Garnett formalism [13]. The typical convergence of the effective parameters as a function of the number of the Fourier components is shown in **Figure 2**. It shows that about 6-7 terms are sufficient to achieve stable solutions.

Once the effective medium parameters for the metamaterial are known, transmission and reflection through the magneto-optical metamaterial can be determined with a standard transfer matrix formalism [22,23].

3. The enhanced Faraday effect

When an external static magnetic field is parallel to the nanorods (axis $\hat{z}$ in Fig. 1) and the effective permittivity tensor of a metamaterial has symmetry shown in Eq. (2b). The eigenmodes supported by the metamaterial represent a combination of elliptically polarized plane waves (see Methods). The dispersion of these modes (the dependence of the components of their wavevector $\vec{k} = \{k_x, k_y, k_z\}$ on angular frequency ω) is given by

$$k_z^2 = \widetilde{\epsilon_\perp}\frac{\omega^2}{c^2} - \frac{k_x^2}{2}\left(\frac{\widetilde{\epsilon_\perp}}{\epsilon_{zz}} + 1\right) \pm \sqrt{\frac{k_x^4}{4}\left(\frac{\widetilde{\epsilon_\perp}}{\epsilon_{zz}} - 1\right)^2 + \gamma_{xy}^2\frac{\omega^2}{c^2}\left(\frac{\omega^2}{c^2} - \frac{k_x^2}{\epsilon_{zz}}\right)} \quad , \qquad (3)$$

where c is speed of light in vacuum (here we use the geometry with $\widehat{xz}$ plane being plane of incidence, resulting in $k_y = 0$). The elliptical polarization of these eigen modes, combined with the difference of their propagating constants, implies that the metamaterial does not preserve the polarization of the linearly polarized incident waves. In general, transmitted monochromatic light has elliptical polarization. For the incident linearly polarized light,

magneto-optical performance is often characterized by the rotation of the major axis of the polarization ellipse of the transmitted light with respect to the linear polarisation of the incident light (the parameter known as rotation of polarization plane $\Delta\theta$; see Methods).

The spectral dependence of polarization rotation in the case of p-polarized incident light with the magnetic field directed along the light propagation has a non-trivial dependence on the angle of incidence (Fig. 3). While the full-wave numerical solutions of the Maxwell equations largely reproduce the spectra of the polarization rotation seen in the experiment (cf Fig. 3a and 3b), the magnitude of the predicted response is several orders of magnitude below what is seen in the experiment. We believe that this disagreement stems from the difference in magneto-optical response between nanostructured and bulk Ni. Indeed, increasing the off-diagonal components of Ni by a factor of 50 with respect to the bulk tabulated data, which assumes saturating static magnetic field [25], brings the results of the simulations in line with the rotation angles seen in the experiment (Fig. 3c).

The effective medium theory developed in this work can be used to drastically reduce the complexity of the numerical solutions of the Maxwell equations. **Figure 4** illustrates the validity of this effective medium theory, described by Eq. (3), in the case when the static magnetic field is directed along the nanorods (both the numerical and the EMT models assume that magneto-optical response of Ni is identical to the values exhibited in bulk samples [25]). The predictions of the effective medium theory adequately describe the results of the full-wave simulations (cf. Fig. 4a and b), at the same time providing drastic reductions in the calculation time and in memory requirements. The spectral dependence of the off-diagonal components of the effective medium polarizability of the Au-Ni-alumina composite for both bulk and the 50-times larger off-diagonal components of Ni susceptibility are shown in Fig. 4c,d. The spectral dependencies of the off-diagonal components of the composite are significantly modified with respect to the spectra for bulk Ni. The change of the sign can even be observed. This is the effect of the interplay between magneto-optical and geometric

anisotropy of the metamaterial. Notably, increasing the magneto-optical response of Ni beyond the tabulated data for bulk Ni film yields the better agreement between the simulated and experimental values for the polarization rotation. In order to avoid excessive fitting of the theoretical model, we limit the theoretical data to a 50-times increase of the off-diagonal response that provides order-of-magnitude agreement with experimental data for both polarization rotation and non-reciprocal transmission. The comparison between experimental and theoretical results indicates that the magneto-optical response of nanostructured Ni is much stronger (approximately 10 times) than that of its bulk counterpart. Indications of this phenomenon have been previously reported in larger-diameter Ni nanowire media with the magneto-optical response ~5 times stronger than that expected from a bulk material response [15,26] and in ultrathin Iron Garnett films [27]. The results suggest that nanostructured Ni can provide further enhancement of magneto-optical response. This results in the significant changes in the cross-polarized transmission due to magneto-optical activity of the composite (Fig. 4e,f). Even in the case when optical response of Ni is considered as in the bulk, the metamaterial provides significant rotation of the polarization plane with the effective Verdet constant of the order of 10^5 [rad/m/T], estimated based on Fig. 3b, 4a, 4b, which is 3 orders of magnitude larger than $\sim 10^2$ [rad/(T · m)] that can be achieved with typical bulk magneto-optical materials, like Terbium Gallium Garnet (TGG) [11].

4. Non-reciprocal transmission

When a static magnetic field is perpendicular to the plane of incidence ($\hat{y}$ direction in geometry shown in Fig. 1), the eigen modes of the metamaterial recover linear polarization, commonly observed in uniaxial crystals. The two families of linearly polarized waves can be grouped in ordinary (s-, TE-polarized) modes that have electric field along the $\hat{y}$ direction and have dispersion

$$k_z^2 = \epsilon_\perp \frac{\omega^2}{c^2} - k_x^2 \qquad (4)$$

and extraordinary (p-, TM-polarized) modes that have the electric field in the $\widehat{xz}$ plane and have the dispersion

$$k_z^2 = \left(\epsilon_\perp - \frac{\gamma_{xz}^2}{\widetilde{\epsilon_{zz}}}\right)\frac{\omega^2}{c^2} - \frac{\epsilon_\perp}{\widetilde{\epsilon_{zz}}}k_x^2 \qquad (5)$$

Quadratic dependence of both families of modes, with both x and z components on the wavevectors, indicate that even in the presence of magneto-optical response the modes of the bulk nanorod metamaterial remain reciprocal. However, a combination of asymmetric geometry, anisotropy, and non-vanishing absorption is expected to yield non-reciprocal excitation of these modes, and, therefore, leads to non-reciprocal transmission of the p-polarized light through the planar slab of the metamaterial [20,21]. Such asymmetric transmission in the metamaterial structure is shown in **Figure 5**. Similar to the cross-polarized transmission described above, the non-reciprocity seen in the experimental data (Fig. 5a) is much stronger than the signal expected from analytical calculations (Fig. 5b).

The validity of the developed effective medium description is illustrated in Figs. 5c,d. The results of the full-wave solutions of Maxwell equations (Fig. 5c) are compared with the EMT predictions (Fig. 5d) in the case where the magneto-optical response of Ni is enhanced 50 times with respect to the tabulated data for bulk materials. Once again, it is seen that such enhancement of the Ni response brings the predictions of both the FEM and EMT models to quantitative agreement with the experiment, further indicating the strong potential effect of nanostructuring of Ni on its magneto-optical properties.

5. Conclusions

We have designed and demonstrated magneto-optical response of plasmonic shelled nanorod metamaterials. Theoretically, we have developed the effective medium technique for understanding the effective magneto-optical response and validated this technique via full-wave solutions of the Maxwell equations. Experimentally, we have demonstrated two

hallmark phenomena enabled by the magneto-optical response of metamaterials, cross-polarization coupling and non-reciprocal transmission. In both cases experimental results indicate that the magneto-optical response of nanostructured Ni is significantly stronger than the tabulated response of its bulk counterpart. While this work focuses on Au/Ni/alumina metamaterials, we expect that qualitatively similar behavior can be obtained in plasmonic/magneto-optic/dielectric core-shell metamaterials with different plasmonic materials (including but not limited to Al, Cu, Ag), different magneto-optical components (Co, Fe), and different dielectrics (including polymers).

The metamaterial approach allows engineering of the magneto-optical response combining magnetic and geometric anisotropy in one metamaterial platform. While concentration of a magnetic material in metamaterial is smaller than in the continuous magnetic film, the enhancement of the response and the lower absorption of the metamaterial, compared to bulk magnetic metals, opens up opportunities for developing new magneto-optical designs. Magneto-optical metamaterial platforms allow the combination of plasmonic and magneto-optical materials in a way to utilize the best qualities of both systems, opening the way for compact high-performance optical isolators and other magneto-optical components.

6. Methods

6.1. Material Fabrication

Plasmonic magnetic metamaterials based on ordered Au-core/Ni-shell nanorod arrays have been fabricated on a glass substrate. Nanoporous anodic alumina oxide (AAO) templates were synthesized by two-step anodization. An aluminium film of 600 nm thickness was deposited on a multilayer glass substrate by magnetron sputtering. The substrate comprised of a glass slide with 20 nm thick adhesive layer of tantalum oxide and a 7 nm thick Au film acting as a weakly conducting layer. Tantalum pentoxide is deposited by sputtering tantalum using a 20%

oxygen/ 80% argon mixture. The porous alumina structures were obtained by a two step-anodization in 0.3 M sulphuric acid at 25V. After an initial anodization process, the poorly ordered porous layer formed was removed by etching in a solution of H_3PO_4 (3.5%) and CrO_3 (20 g l^{-1}) at 70°C. An ordered, patterned surface was obtained after removal of the porous layer formed during first step of anodization. Then the samples were anodized again under the same conditions as in the first step. The anodized samples were subsequently etched in 30 mM NaOH to achieve pore widening and remove the barrier layer.

Gold electrodeposition was performed with a three electrodes system using a non-cyanide solution. The length of the nanorods was controlled by the electrodeposition time. The sample was etched again in 30 mM NaOH to form nanoshells around the Au nanorods. The thickness of the Ni shell around the Au nanorods was controlled by etching time. Nickel was electrodeposited in these nanoshells using a mixed solution of 0.2M Nickel sulphate and 0.1M boric acid.

The structure used in these measurements has an Au core of 30 nm in diameter and a Ni shell 8±2 nm thick. The period is 64 nm and length of nanorods is 200 nm.

6.2. Optical Characterization

The schematic diagram of experimental set up for optical measurements is shown in **Figure 6**. It consists of a white light source, collimation lenses, a polarizer and an analyzer, with optical axes that can be adjusted with respect to each other and the plane of incidence, and a CCD-based spectrometer. The sample is mounted onto a non-magmatic stage. Neodymium ring and disc magnets of 20 mm diameter and 10 mm thickness with magnetic field of 0.3T and 0.16T, respectively, are used in the experiments to provide a magnetic field. The magnets are adjusted at the distance of 5 mm from the sample to maximize the magnetic field strength. The external magnetic field is applied horizontally along the direction of the incident light (the magnetic field has the components both along and perpendicular to the nanorods, along

both ordinary and extraordinary axes of the metamaterial, the ratio of the components depends on the angle of incidence) or, alternatively, from the top of the sample perpendicular to the direction of the incident light (the magnetic field perpendicular to the nanorod axes, along the ordinary axis of the metamaterial). The size of the magnets is much larger than the diameter of the optical beam, so that uniform magnetic field can be assumed across the illuminated spot. The measurements are performed in transmission configuration in the saturated magnetic field. The samples are fully demagnetized for the baseline measurements. In order to retrieve the polarization of the transmitted light, the intensity $P(\theta)$ of the light is measured at 4 different analyzer angles ($\theta = 0°$, 30°, 45° and 60° with respect to the incident polarizer angle). We use these four measurements and the fact that that $P(\theta) \propto |\boldsymbol{E}.\boldsymbol{u}(\boldsymbol{\theta})|^{\mathbf{2}}$, where $\boldsymbol{u}(\boldsymbol{\theta})$ is the unit vector along the analyser direction, to determine the 3 unknown quantities of the transmitted polarization state $\boldsymbol{E} = (E_o^{re}, E_e^{re} + iE_e^{im})$ using a least squared error fit [28]. The rotation due to the introduction of the magnetic field can then be determined by comparing the angle of orientation of the major semiaxis of the polarization ellipse.

6.3. The effective medium analysis

As mentioned above, the effective permittivity is calculated in quasi-static approximation, with spatial distribution of electric field given by the electric potential ($\vec{E} = -\vec{\nabla}\Phi$) that, in turn, is given by Eq. (1). Symmetry of the problem dictates that only odd Fourier modes ($m = 1,3,\dots,M$) contribute to the solution.

To find the amplitudes of coefficients α_i and β_i , we use boundary conditions at each inter-shell boundaries to relate the coefficients in the neighboring layers, using interface-specific scattering and transfer matrices

$$\begin{bmatrix} \overrightarrow{\alpha_i^-} \\ \overrightarrow{\beta_i^-} \end{bmatrix} = \widehat{S}_i \begin{bmatrix} \overrightarrow{\alpha_i^+} \\ \overrightarrow{\beta_i^+} \end{bmatrix}$$

$$\begin{bmatrix} \overrightarrow{\alpha_{i-1}^{+}} \\ \overrightarrow{\beta_{i-1}^{+}} \end{bmatrix} = \widehat{T_i} \begin{bmatrix} \overrightarrow{\alpha_i^{+}} \\ \overrightarrow{\beta_i^{+}} \end{bmatrix} . \quad (6)$$

On the implementation level, the matrices depend on the direction of the external static magnetic field. In particular, for the case of B_z field, the S and T matrices for a particular interface, can be obtained by enforcing the boundary conditions for the electric field and the displacement at this interface. Given a general form of the potential [Eq. (1)] as well as cylindrical symmetries of nanorod shells, the relevant boundary conditions reduce to continuity of tangential electric field (E_ϕ) and normal electric displacement (D_r). Cylindrical symmetry of nanorod shells allows one to decouple the coefficients related to the Fourier harmonics corresponding to different indices m from each other. It becomes convenient to represent the boundary conditions in a matrix form

$$\widehat{F_{i-1}(r_i)} \begin{pmatrix} \overrightarrow{\alpha_{i-1}^{+}} \\ \overrightarrow{\beta_{i-1}^{+}} \\ \overrightarrow{\alpha_{i-1}^{-}} \\ \overrightarrow{\beta_{i-1}^{-}} \end{pmatrix} = \widehat{F_i(r_i)} \begin{pmatrix} \overrightarrow{\alpha_i^{+}} \\ \overrightarrow{\beta_i^{+}} \\ \overrightarrow{\alpha_i^{-}} \\ \overrightarrow{\beta_i^{-}} \end{pmatrix} , \quad (7)$$

where matrices $\widehat{F_i(r_j)}$ have $4M$ rows and columns each. The m-th ($2M + m$-th) bi-rows of the matrix represent the electric field (displacement) for the terms preserving particular $\sin(m\phi), \cos(m\phi)$ terms in the i-th layer at the position r_j. Eq. (7) can be straightforwardly transformed into

$$\begin{pmatrix} \overrightarrow{\alpha_{i-1}^{+}} \\ \overrightarrow{\beta_{i-1}^{+}} \\ \overrightarrow{\alpha_{i-1}^{-}} \\ \overrightarrow{\beta_{i-1}^{-}} \end{pmatrix} = \widehat{M_i} \begin{pmatrix} \overrightarrow{\alpha_i^{+}} \\ \overrightarrow{\beta_i^{+}} \\ \overrightarrow{\alpha_i^{-}} \\ \overrightarrow{\beta_i^{-}} \end{pmatrix} , \quad (8)$$

where $M_i = \widehat{F_{i-1}(r_i)}^{-1} \widehat{F_i(r_i)}$. As before, matrix M is a $4M \times 4M$ matrix. It can be represented as four sub-matrices, M_i^{jk} $2M \times 2M$ each, with $j, k = 1,2$. It is now easy to represent the S_i, T_i matrices in terms of the sub-matrices M_i^{jk} and S_{i-1}:

$$S_i = -(M_i^{22} - S_{i-1} M_i^{12})^{-1} (M_i^{21} - S_{i-1} M_i^{11})$$

$$T_i = M_i^{11} + M_i^{12} S_i \,. \qquad (9)$$

Eq. (9), combined with requirement to have finite field at the origin ($\widehat{S_1} = \hat{0}$) solves the problem of finding the full set of interface-specific matrices $\widehat{S_\iota}$ and $\widehat{T_\iota}$ for the case when the external magnetic field is parallel to the nanorods.

In the complimentary case, when the static magnetic field is directed along the $\hat{y}$ direction, symmetry of the permittivity of components of metamaterial is represented by Eq. (2a). Therefore, the $m = 1$ components of the in-plane fields are coupled to the z-field. The boundary conditions now require continuity of both E_ϕ, and D_r (for all values of m) as well as continuity of E_z (for $m = 1$). With these additions, the procedure for calculating$\widehat{S_\iota}$ and $\widehat{T_\iota}$ matrices is similar to the one described above. The resultant set of matrices $\widehat{S_\iota}$ and $\widehat{T_\iota}$ can be used to calculate response of the individual multi-shelled nanorod (or a set of periodic rods) to any quasi-static external electric field. To analyze effective medium behavior of the metamaterial, we assume a homogeneous excitation field (given by $\alpha_N^1 = 1$) and impose periodic boundary conditions on the fields across the unit cell. To achieve the latter goal, we chose a sufficiently large number of points x_p, y_p along the unit cell boundary (it can be shown that the symmetry imposed by the choice of the Fourier harmonics suffices to restrict these points to the first quadrant of the boundary where $x_p, y_p > 0$) and represent the distribution of the Cartesian component of the field $E_\xi(x_p, y_p)$ with $\xi = x, y$ and the coefficients $\overrightarrow{\alpha^{\pm}}$ and $\overrightarrow{\beta^{\pm}}$ in the matrix form, $\hat{\mathcal{E}}\begin{bmatrix}\overrightarrow{\alpha_N^+}\\ \overrightarrow{\beta_N^+}\end{bmatrix}$, where each row of the matrix $\hat{\mathcal{E}}$ corresponds to a particular combination of ξ and p, and each column of the matrix corresponds to the contribution of the individual $\sin(m\phi)$ or $\cos(m\phi)$ term to the field. In the limit $p > M$, this matrix reduces the field periodicity condition to an overdetermined least-square fit problem that is used to find all the coefficients $\overrightarrow{\alpha_\iota}$ and $\overrightarrow{\beta_\iota}$ except for α_N^1.

6.4. Dispersion and polarization of plane waves in magneto-optical materials

In non-magnetic media (materials with relative magnetic permeability $\mu_r = 1$), the Maxwell's equations result in

$$\vec{\nabla} \times \vec{\nabla} \times \vec{E} = -\frac{1}{c^2}\frac{\partial^2}{\partial\, t^2}\hat{\epsilon}\vec{E} \quad . \qquad (10)$$

Assuming plane-wave solution, $\vec{E} = \overrightarrow{E_0}\exp(i\vec{k}\cdot\vec{r} - i\omega t)$, the above equation reduces to eigen-value problem

$$\vec{k}\cdot\left(\vec{k}\cdot\overrightarrow{E_0}\right) - \left(\vec{k}\cdot\vec{k}\right)\overrightarrow{E_0} + \frac{\omega^2}{c^2}\hat{\epsilon}\overrightarrow{E_0} = 0 \qquad (11)$$

that can be used to find the dispersion (a dependence of components of the wavevector $\vec{k}$ on a frequency ω) as well as the polarization (relationship between components of the field amplitude $\overrightarrow{E_0}$) of the eigen modes of the system [19]. In particular, when the symmetry of the permittivity is given by Eq. (2a), Eq. (11) in the limit $\vec{k} = \{k_x, 0, k_z\}$ yields

$$\begin{pmatrix} \epsilon_\perp\frac{\omega^2}{c^2} - k_z^2 & 0 & i\gamma_{xz}\frac{\omega^2}{c^2} + k_x k_z \\ 0 & \epsilon_\perp\frac{\omega^2}{c^2} - k_x^2 - k_z^2 & 0 \\ -i\gamma_{xz}\frac{\omega^2}{c^2} + k_x k_z & 0 & \widetilde{\epsilon_{zz}}\frac{\omega^2}{c^2} - k_x^2 \end{pmatrix}\begin{pmatrix} E_{0x} \\ E_{0y} \\ E_{0z} \end{pmatrix} = 0 \quad . \qquad (12)$$

The dispersion of the eigenmodes are given by Eqs. (4,5), while eigen polarizations are given by $\overrightarrow{E_0} = \{0,1,0\}$, representing s-polarized wave, Eq. (4)] and $\overrightarrow{E_0} = \left\{1,0,-\frac{\epsilon_\perp - k_z^2\, c^2/\omega^2}{i\gamma_{xz} + k_x k_z\, c^2/\omega^2}\right\}$, representing p-polarized waves. Note that both eigenmodes are linearly polarized.

Similarly, when the symmetry of the permittivity is given by Eq. (2b), we obtain

$$\begin{pmatrix} \widetilde{\epsilon_\perp}\frac{\omega^2}{c^2} - k_z^2 & i\gamma_{xy}\frac{\omega^2}{c^2} & k_x k_z \\ -i\,\gamma_{xy}\frac{\omega^2}{c^2} & \widetilde{\epsilon_\perp}\frac{\omega^2}{c^2} - k_x^2 - k_z^2 & 0 \\ k_x k_z & 0 & \epsilon_{zz}\frac{\omega^2}{c^2} - k_x^2 \end{pmatrix}\begin{pmatrix} E_{0x} \\ E_{0y} \\ E_{0z} \end{pmatrix} = 0\,, \qquad (13)$$

resulting in the dispersion equation of the form Eq. (3) and the amplitude of the eigen modes given by $\overrightarrow{E_0^+} = \left\{-i\frac{\widetilde{\epsilon_\perp}\frac{\omega^2}{c^2} - k_x^2 - k_z^2}{\gamma_{xy}\frac{\omega^2}{c^2}}, 1, E_{0z}^+\right\}$, $\overrightarrow{E_0^-} = \left\{1, i\frac{\gamma_{xy}\frac{\omega^2}{c^2}}{\widetilde{\epsilon_\perp}\frac{\omega^2}{c^2} - k_x^2 - k_z^2}, E_{0z}^-\right\}$, with $E_{0z}^\pm =$

$-\frac{k_x k_z}{\widetilde{\epsilon_\perp}\frac{\omega^2}{c^2}-k_x^2} E_{0x}^{\pm}$. In the limit of vanishing magneto-optical response ($\gamma_{xy} = 0$), we recover two linear- s- ($E_{0y} \neq 0$) and p-polarized ($E_{0x}, E_{0z} \neq 0$) waves. When $\gamma_{xy} \neq 0$, both eigenmodes however are elliptically polarized.

6.5. Numerical solutions of the Maxwell equations

To verify the validity of the developed effective medium theory, transmission and reflection of the composites were calculated with three-dimensional vectorial solutions of the Maxwell equations with a commercial FEM solver [24]. The model explicitly considers a single (finite height) unit cell of a metamaterial and implements the Floquet periodicity along x- and y-directions (representing in-plane wavenumber of the incident plane wave) to mimic the infinite planar structure. In the z-direction, the geometry is terminated with two ports at the bottom and two ports at the top interfaces, assuring the reflection-less transmission of co- and cross-polarized light. A subwavelength unit cell of the metamaterial, along with wavelength-scale separation between the ports and the nanorod, ensures that no diffracted beam contributes to the field at the location of the ports. Transmission and reflection can be extracted directly from the FEM model using S-parameter calculations.

In separate calculations the metamaterial was approximated as a homogeneous slab with the effective permittivity tensor given by Eq. (1), and the optical response of the planar metamaterial layer was calculated using the transfer-matrix-method (TMM)-based formalism. Our in-house implementation of TMM is available as a sub-class of rigorous coupled wave analysis packet (Supporting Information).

In order to calculate rotation of the polarization plane, the transmitted part of a normally-incident light is represented as a linear combination of TE- and TM-polarized plane waves with amplitudes a_y and a_x, respectively. This combination represents, in general,

elliptically polarized light. The rotation of polarization represents the direction of the major semiaxis of the ellipse, given by

$$\theta = \frac{1}{2}\arg\frac{a_x - i\,a_y}{a_x + i\,a_y} \quad . \quad (14)$$

Supporting Information
Supporting Information in the form of the Matlab implementation of the effective medium theory for shelled nanorod metamaterials is available from the Wiley Online Library and from the author.

Acknowledgements
This research has been supported by the US Army Research Office (grant# W911NF-16-1-0261), EPSRC (UK) and the ERC iPLASMM project (No. 321268). A.Z. acknowledges support from the Royal Society and the Wolfson Foundation.

B. Fan and M. Nasir contributed equally to this work.

Received: ((will be filled in by the editorial staff))
Revised: ((will be filled in by the editorial staff))
Published online: ((will be filled in by the editorial staff))

References

1. S. Sugano, N. Kojima (eds), Magneto Optics, Springer (Berlin, 2000)
2. D. Jalas, A. Petrov, M. Eich, W. Freude, S. Fan, Z. Yu, R. Baets, M. Popović, A. Melloni, J.D. Joannopoulos, M. Vanwolleghem, C.R. Doerr, H. Renner, *Nat. Photon.* **2013**, *7*, 579
3. A.B. Khanikaev, G. Shvets, *Nat. Phot.* ***2017***, *11*, 763
4. Z. Yu, G. Veronis, Z. Wang, S. Fan, *Phys. Rev. Lett.* **2008**, *100*, 023902
5. M. Sadatgol, M. Rahman, E. Forati, M. Levy, D. Ö. Güney, *J. Appl. Phys.* **2016**, *119*, 103105

6. P. Ginzburg, F. J. Rodríguez Fortuño, G. A. Wurtz, W. Dickson, A. Murphy, F. Morgan, R. J. Pollard, I. Iorsh, A. Atrashchenko, P. A. Belov, Y. S. Kivshar, A. Nevet, G. Ankonina, M. Orenstein, A. V. Zayats, *Opt. Expr.* **2013**, *21*, 14907

7. D. Vestler, I. Shishkin, E. A. Gurvitz, M. E. Nasir, A. Ben-Moshe, A. P. Slobozhanyuk, A. V. Krasavin, T. Levi-Belenkova, A. S. Shalin, P. Ginzburg, G. Markovich, A. V. Zayats, *Opt. Expr.* **2018**, *26*, 17841

8. M. E. Nasir, W. Dickson, G. A. Wurtz, W. P. Wardley, A. V. Zayats, *Adv. Mat.* **2014,** *26*, 3532

9. V. Drachev, V. A. Podolskiy, A. Kildishev, *Opt. Expr.* **2013**, *21*, 15048

10. A. Poddubny, I. Iorsh, P. Belov, Y. Kivshar, *Nat. Photon.* **2013**, *7*, 948

11. D. J. Dentz, R. C. Puttbach, R. F. Belt, *AIP Proc.* **1974**, 18954

12. R. Wangberg, J. Elser, E. E. Narimanov, V. A. Podolskiy, *J. Opt. Soc. Amer*. **2006**, *B23*, 498

13. B. Wells, W. Guo, V. A. Podolskiy, *MRS Commun*. **2016**, *6*, 23

14. W. T. Perrins, D. R. McKenzie, R. C. McPhedran, *Proc. R. Soc. Lond*. **1979**, *A369*, 207

15. S. Melle, J. Menendez, C.Armelles, D. Naas, M. Vazquez, K. Nielsch, *Appl. Phys. Lett.* **2003**, *83*, 4547

16. P. M. Hui, D. Stroud, *Appl. Phys. Lett.* **1987**, *50*, 950

17. H. K. Krishnamoorthy, Z. Jacob, E. Narimanov, I. Kretzschmar, V. M. Menon, *Science*, **2012**, *336*, 205

18. P. Ginzburg, D. Roth, M.E. Nasir, P. Segovia Olvera, A.V. Krasavin, J. Levitt, L.M. Hirvonen, B. Wells, K. Suhling, D. Richards, V.A. Podolskiy, A.V. Zayats, *Light: Sci. Appl.* **2017**, *6*, e16273

19. L.D. Landau, E.M. Lifshitz and L.P. Pitaevskii, Electrodynamics of Continuous Media, Landau and Lifshitz Course of Theoretical Physics, Vol. 8, Reed Educ. Pub. (Oxford, UK, 1980)

20. V.A. Fedotov, P.L. Mladyonov, S.L. Prosvirnin, A.V. Rogcheva, Y. Chen, N.I. Zheludev, *Phys. Rev. Lett*. **2006**, *97*, 167401

21. A. Leviyev, B. Stein, A. Christofi, T. Galfsky, H. Krish-namoorthy, I. L. Kuskivsky, V. Menon, A. B. Khanikaev, *APL Photon*. **2017**, *2*, 076103

22. S. M. Rytov, *Sov. Phys. JETP*, **1956**, *2*, 466

23. P. Yeh, A. Yariv, and C.-S. Hong, *J. Opt. Soc. Amer*. **1977**, *67*, 423

24. Comsol Multiphysics, COMSOL AB, www.comsol.com

25. G. S. Krinchik, V. A. Artem'ev, *Sov. Phys. JETP*, **1968**, *26*, 1080

26. A. A. Stashkevich, Y. Roussigné, A. N. Poddubny, S.-M. Chérif, Y. Zheng, F. Vidal, I. V. Yagupov, A. P. Slobozhanyuk, P. A. Belov, Y. S. Kivshar, *Phys. Rev*. **2015**, *B92*, 214436

27. M. Levy, A. Chakravarty, H.-C. Huang, R. M. Osgood Jr., *Appl. Phys. Lett*. **2015**, *107*, 011104

28. L. Nicholls, F. J. Rodríguez-Fortuño, M. E. Nasir, R. M. Cordova-Castro, N. Olivier, G. A. Wurtz, A. V. Zayats, *Nat. Photon.* **2017**, *11*, 628

29. G. Milton, Theory of composites, Cambridge U. Press (Cambridge, UK, 2002)

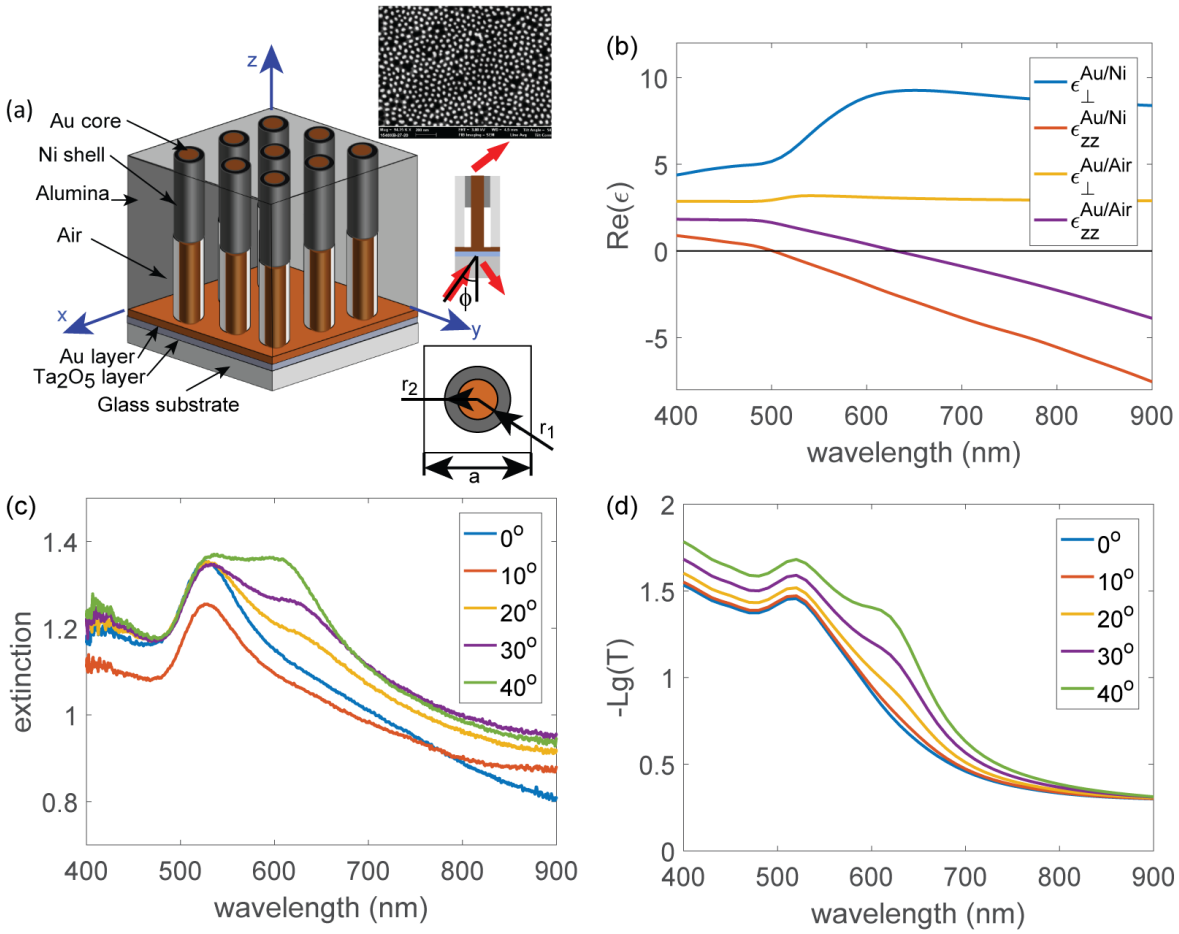

Figure 1. (a) Schematic geometry and the SEM image (top inset) of the nanorod composite. (b) Diagonal components of the effective permittivity tensor of Au/Ni/Al_2O_3 and Au/air/Al_2O_3 metamaterials. (c,d) Optical extinction spectra of the Au/Ni/Al_2O_3 metamaterial excited with *p*-polarized light for different angles of incidence: (c) experiment and (d) EMT calculations.

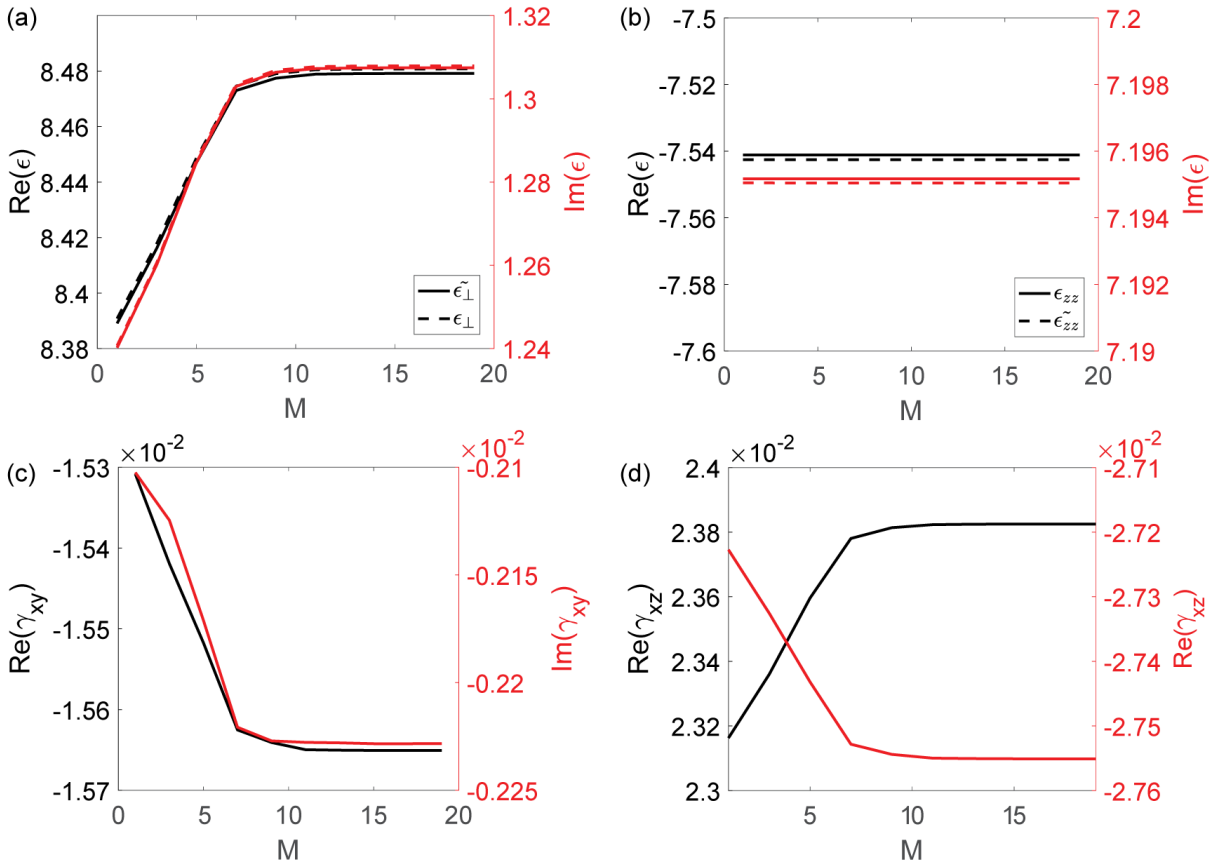

Figure 2. Convergence of the effective medium parameters as a function of a number of terms in Eq. (1). Geometric parameters of the unit cell are $a = 64\ nm, r_1 = 15\ nm,$ and $r_2 = 23\ nm,$ and the permittivity of the components are $\epsilon_1 = -34.47 + 7.94i, \epsilon_2 = -14.7 + 24.98i,$ and $\epsilon_3 = 3.09$, with magneto-optical response of Ni given by $i\gamma_{Ni} = -0.36 + 0.126i$.

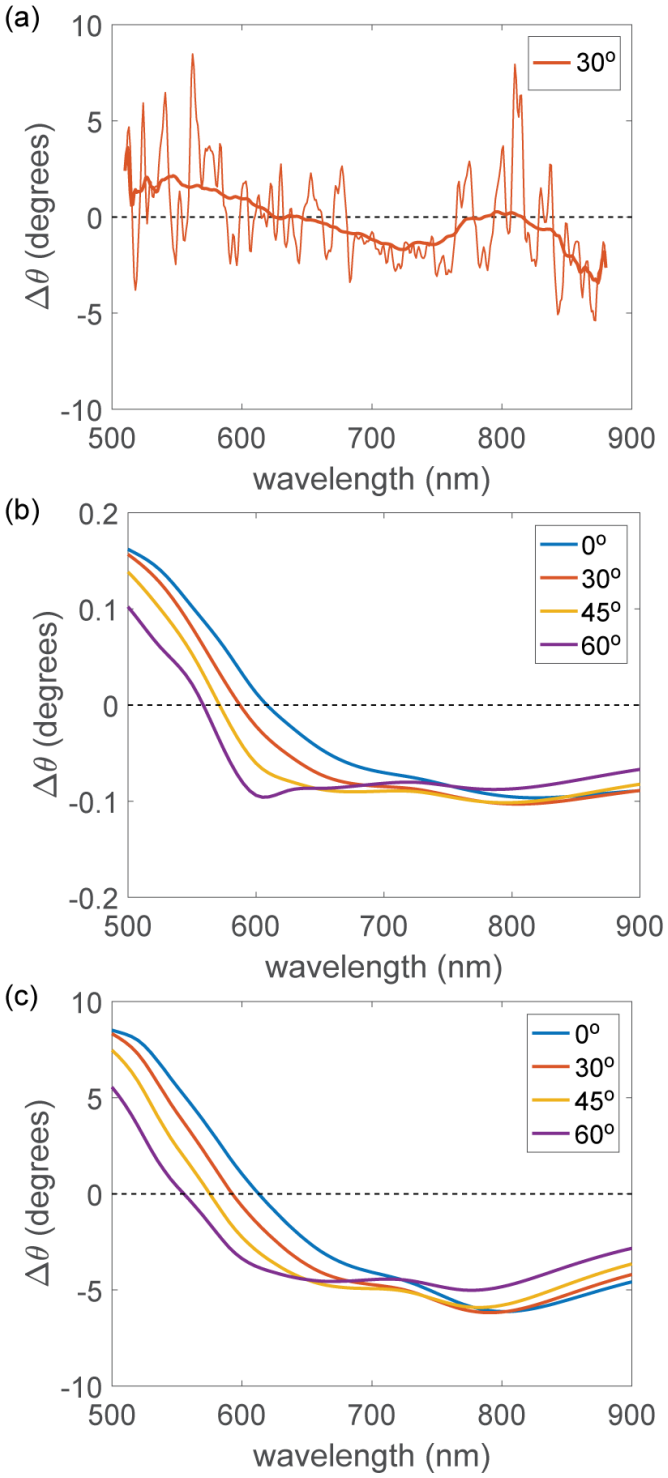

Figure 3 Rotation of the polarization plane of p-polarized light incident on the metamaterial at different angles of incidence when static magnetic field is directed along the direction of incident light: (a) experimental data for an angle of incidence of 30° averaged by applying Savitzky–Golay filter (thick line) to increase signal-to-noise ratio (please note that due to the high extinction, the experimental signal is weak for wavelengths below approximately 550 nm, preventing accurate reconstruction of polarisation state); (b), (c) numerical simulations for bulk tabulated Ni permittivity (b) and for the off-diagonal permittivity components increased 50 times (c).

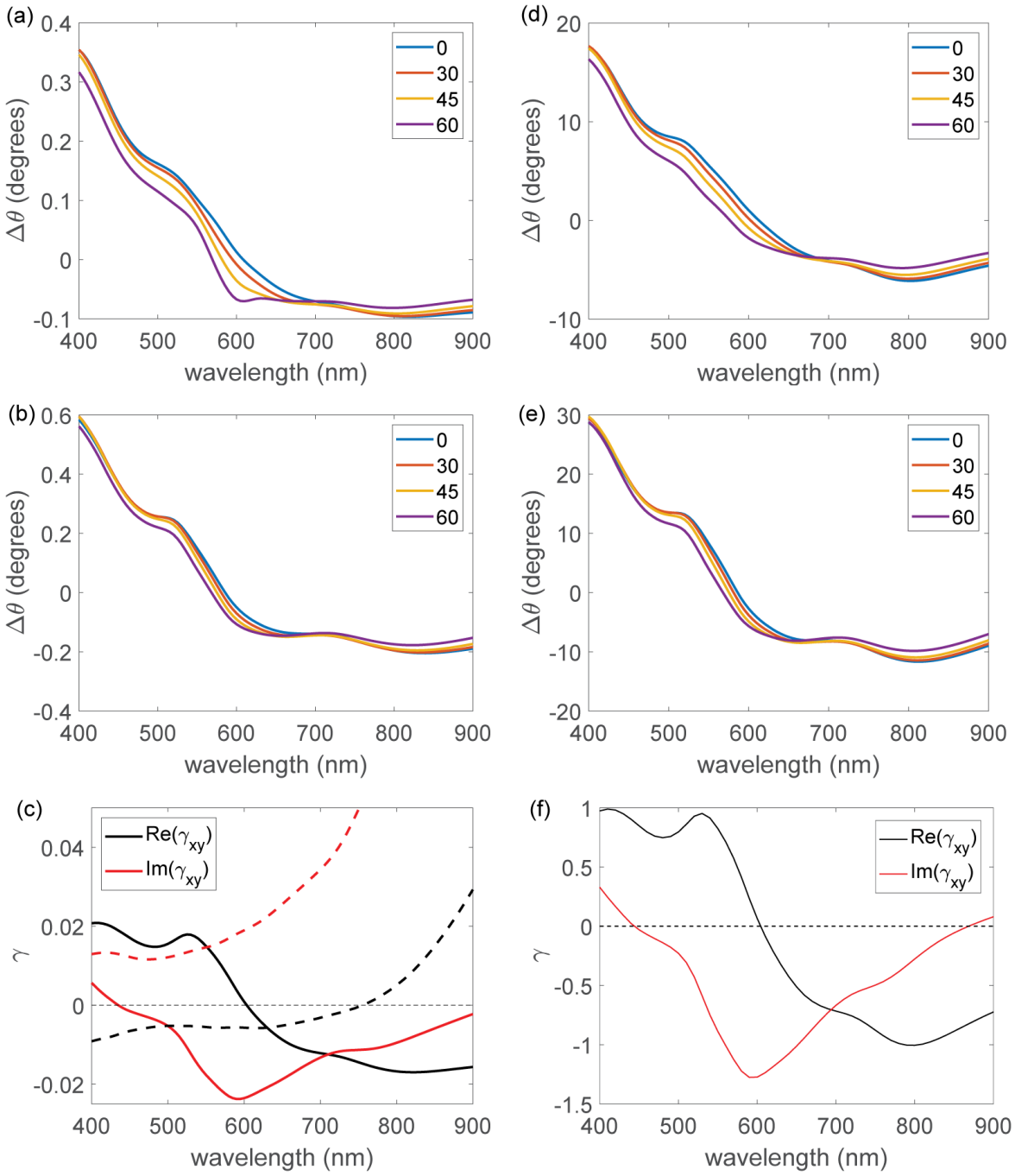

Figure 4. (a,b,d,e) Rotation of the polarization plane for a p-polarized beam incident on the metamaterial at different angles of incidence when static magnetic field is along the nanorods: (a,d) FEM and (b,e) EMT simulations. (c,f) The spectral dependences of the off-diagonal components γ_{xy} used in (b,d), respectively: (solid lines) the off-diagonal components of the effective permittivity tensor, (dashed lines) the off-diagonal components of Ni, scaled by the volumetric concentration of Ni in the composite. Tabulated data for Ni [25] are assumed in (a-c), while γ_{xy} for Ni increased 50 times with respect to the tabulated data is assumed in (d-f).

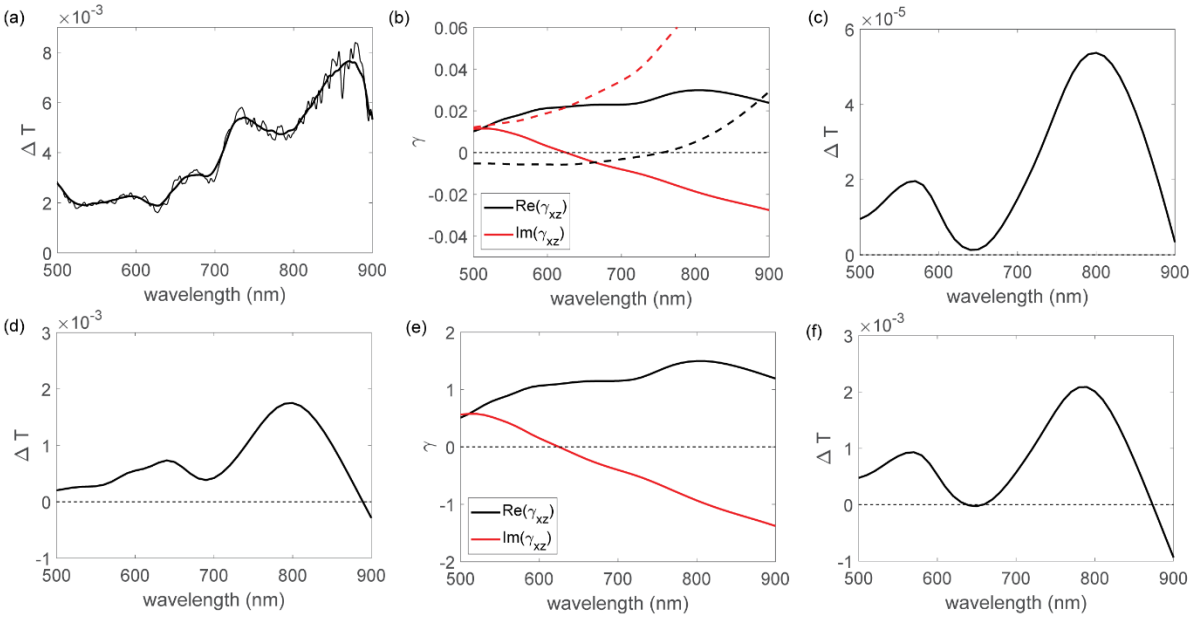

Figure 5. Non-reciprocal transmission of a p-polarized light incident at 30° when static magnetic field is perpendicular to the plane of incidence: (a) experimental data for an angle of incidence of 30° averaged by applying Savitzky–Golay filter (thick line) to increase signal-to-noise ratio (please note that due to the high extinction, the experimental signal is weak for wavelengths below approximately 550 nm), (c,f) TMM and (d) FEM simulations for (c) the tabulated data for Ni [25] and (d,f) γ_{xz} for Ni increased 50 times with respect to the tabulated data. Solid lines in (b,e) are the spectra of the off-diagonal components γ_{xz} of the effective permittivity for the TMM calculations in (c,d). Dashed lines in (b) are the spectra of the off-diagonal components γ_{xz} of the permittivity tensor of Ni scaled by the volumetric concentration of Ni in the composite.

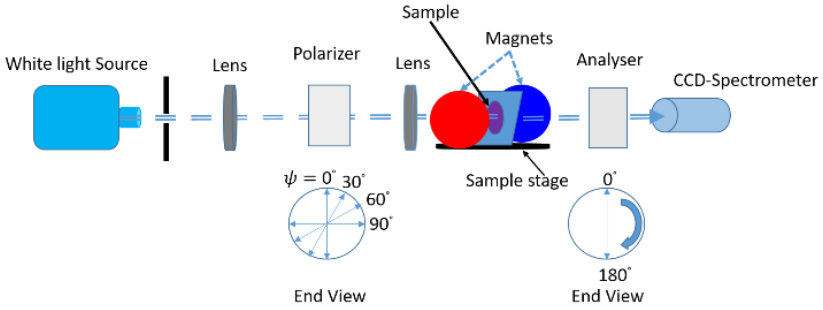

Figure 6. Experimental setup. Bottom diagrammes shows the orientation of the polarizer and analyser for MO measurements.

A new type of a hyperbolic magneto-optical metamaterial based on Au-Ni nanorod arrays is developed. The metamaterial exhibits the enhanced magneto-optical response with large rotation of a polarization plane and nonreciprocal light transmission. Response of metamaterial is drastically enhanced with respect to bulk ferromagnetic media due to an interplay between strong anisotropy and magnetic-field induced polarization rotation.

Keyword: **metamaterials, nonreciprocity, Faraday effect, effective medium theory**

Bo Fan, Mazhar E. Nasir, Anatoly V. Zayats, and Viktor A, Podolskiy*

Magneto-optical metamaterials: Nonreciprocal transmission and Faraday effect enhancement

ToC figure

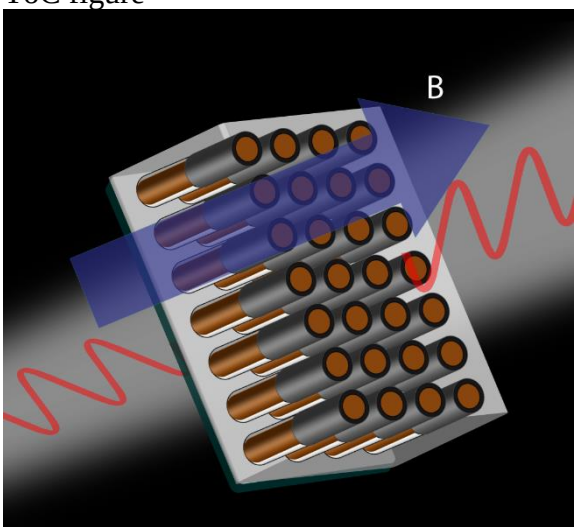

Supporting Information

Magneto-optical metamaterials: Nonreciprocal transmission and Faraday effect enhancement

Bo Fan, Mazhar E. Nasir, Anatoly V. Zayats, and Viktor A, Podolskiy**

Supporting information comprises a set of Matlab-based source files demonstrating numerical implementation of the effective medium theory, producing Figure 2.